Interactions between Estuaries, Coastal Seas and Shelf Seas, Ed. T. Yanagi, pp. 37–55.

Direct Measurement of Turbulence Properties by a BB-ADCP in Bottom Boundary Layer

R. T. CHENG, C.-H. LING and J. W. GARTNER

Water Resources Division, U.S. Geological Survey, Menlo Park, CA 94025, U.S.A.
e-mail: rtcheng@usgs.gov

Abstract. Broad-band acoustic Doppler current profilers (BB-ADCPs), in high resolution modes, have been shown to be very effective for studies of turbulent mean flow properties in the marine bottom boundary layer. The BB-ADCP is capable of measuring the velocity distribution in the bottom boundary layer, providing about 20–30 velocity points within 1.5 m from the sediment-water interface at a sampling rate slightly above 1 Hz. In this study, the potential of the high frequency sampling scheme of the BB-ADCP is explored. By saving single-ping velocity measurements, the turbulence properties of the bottom boundary layer can be extracted from these measurements. Specifically, the high frequency velocity profiles are analyzed leading to direct measurements of turbulence properties of a bottom boundary layer in South San Francisco Bay, California. The objectives of this study are: 1) to explore techniques of measuring turbulence properties by a BB-ADCP; 2) to determine the Reynolds stress distribution in the bottom boundary layer from correlation of high frequency velocity components; 3) to compare the Reynolds stress with the bottom boundary layer properties deduced by conventional methods; and 4) to characterize the rate of vertical mixing in the water column based on these measurements. This investigation is moderately successful; some limitations of this approach have been identified for future consideration of improvements.

INTRODUCTION

The mechanisms that control the transport, erosion and deposition of fine sediments, and the mechanisms that control the mixing in tidal estuaries are directly influenced by the highly variable hydrodynamic conditions and turbulence properties near the bed. In order to determine the hydrodynamic characteristics, using a few (4~6) current meters is not sufficient to resolve the high velocity gradients (shear) in the bottom boundary layer. Recently, Cheng *et al.* (1997, 1998, 1999) have successfully used high resolution broad band acoustic Doppler current profilers (BB-ADCPs) to obtain detailed measurements of the turbulent mean velocity distribution in the bottom boundary layer starting at about 10 cm from the bed in 5 cm increments to approximately 1.5 m. These high-resolution velocity profiles are then used for estimates of friction velocity, u_*, and bottom roughness length, z_0. The shear stress near bed directly affects conditions conducive for sediment erosion or deposition, transport, and vertical mixing. Furthermore, the hydrodynamic properties in the bottom boundary layer define

the relations among tidal velocity, bottom shear stress (friction velocity), and sediment bed roughness. A global method for estimating friction velocity, u_*, (or bottom shear stress) and bottom roughness length, z_o, has been proposed by Cheng *et al.* (1999) and shown to be effective. Using the global method, more consistent estimates of roughness length and friction velocity have been achieved. With these boundary layer properties, a correlation among bed roughness length (z_o), drag coefficient, friction velocity, (u_*), and tidal velocity outside of the boundary layer (reference velocity) has been established (Cheng *et al.*, 1999).

In the aforementioned applications, BB-ADCPs are used to determine turbulent mean flow properties in the bottom boundary layer. For each velocity profile measurement, many single-ping velocity profiles are taken (on the order of 40–60), and the mean flow properties are computed and recorded within the instrument. The single-ping velocity profiles are not saved. Alternatively, it is also possible to record each single-ping velocity profile for post deployment processing. In this high frequency sampling strategy, the resulting measurements can be averaged to recover all mean flow properties, and the high frequency data can be analyzed to extract turbulence properties. The only downside of this approach, for self-contained instrument deployment, is that the data file becomes enormously large. Thus the capacity of the instrument recorder becomes a limiting factor that restricts the length of field deployment. This high frequency ADCP sampling strategy has been used in investigations of turbulence in tidal channels with some degree of success by Stacey (1997), Lueck and Lu (1997), and Lu (1998).

Based on previous successful usage of BB-ADCP for mean flow measurements, and in continuing pursuit of a better understanding of the turbulence properties and hydrodynamics in the bottom boundary layer in tidal estuaries, BB-ADCPs were again used in this investigation. Two ADCPs were deployed on a bottom platform with acoustic transducers pointing vertically down. Both ADCPs were programmed to function in high-resolution mode and using high frequency data sampling strategy. The main objectives of the present study are to explore the usefulness of using BB-ADCP for measuring both the mean flow and turbulence properties, and to determine instrument limits in high frequency flow measurements in the bottom boundary layer. As a validation for the present approach, the Reynolds stress deduced from high frequency ADCP data will be compared with properties deduced from mean flow. Furthermore, other turbulence variables such as eddy viscosity distribution and total turbulent kinetic energy distribution in the bottom boundary layer will be estimated. More importantly, any weakness found in this approach will be the basis for consideration in future studies using BB-ADCP for turbulence measurements in the bottom boundary layer of bays and estuaries.

FIELD EXPERIMENTS

Modes of BB-ADCP

The BB-ADCPs used in this study are RD Instruments (RDI), model SC-1200 which utilize four acoustic transducers oriented 90 degrees apart. The

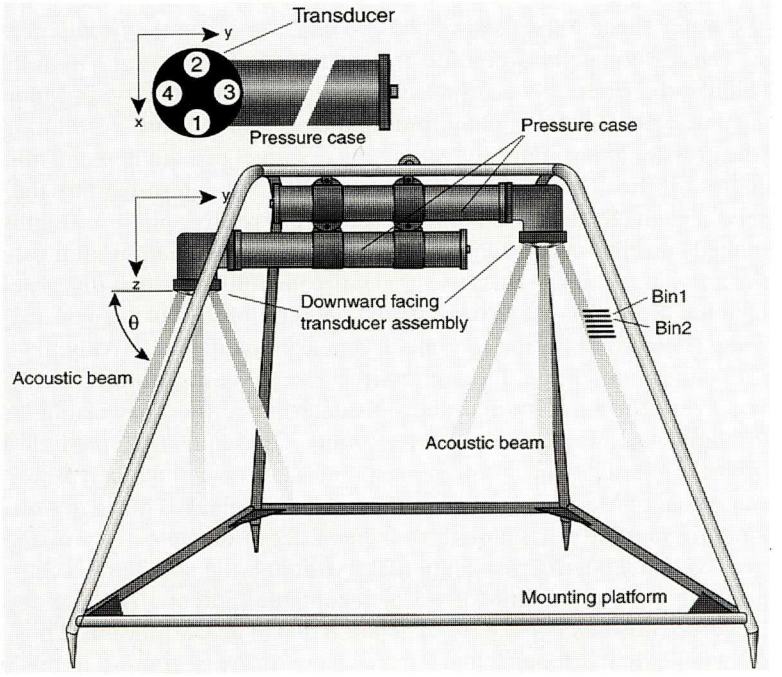

Fig. 1. Schematic diagram of two bottom mounted, downward pointing BB-ADCPs, and the orientation and naming convention of the acoustic beams in relation to the right-handed earth Cartesian coordinates (x, y, z).

resulting acoustic beams are transmitted 20 degrees from vertical and have a transmit frequency of 1228.8 kHz, Fig. 1. One of the units has a fifth beam which is oriented vertically. The water velocities along the acoustic beams are determined from relations between the transmitted and echoed acoustic signals either by Doppler frequency shift (narrow band) or by coherence (broad band). Basic trigonometric relations convert the along-beam velocity measurements into three orthogonal velocity components referenced to earth coordinates. A velocity profile is determined by sampling the reflected (echoed) acoustic signals at discrete time intervals that correspond to depth intervals (called bins). In practice, about 6% of the water column immediately adjacent to an abrupt interface (water surface or sediment bed) cannot be sampled accurately because of parasitic acoustic side lobes that interfere with primary acoustic signals (Gordon, 1996).

The BB-ADCP has a choice of two high-resolution modes, Mode-5 and Mode-8, provided by the manufacturer (RD Instruments, 1997). In both modes, pulse-to-pulse coherence principle is used for signal processing (Lohrmann *et al.*, 1990; Lhermitte and Lemmin, 1994). For BB-ADCP, one of the limitations in high-resolution modes is that the double pulsed signals can "de-correlate" because of the long pulse-lag. For a 1200 KHz instrument, signals de-correlate

when the water speed exceeds about 45~50 cm/s, or when the turbulence is too intense. The difference between Mode-5 and Mode-8 operations is in the way with which correlation information is used to determine velocity. In Mode-5, an ambiguity velocity is estimated by finding the peak in the auto-correlation from the whole profile. This ambiguity velocity is assigned to a bin near the middle of the velocity profile. The remaining velocity profile is determined by the phase difference at each bin and the ambiguity velocity to resolve phase ambiguities. If the averaged correlation coefficient is below a pre-assigned minimum value, the signals are de-correlated. In this case, the entire velocity profile is discarded. The advantage for Mode-5 is when a measured velocity profile is deemed valid, the single-ping standard deviation for velocity measurement is relatively low, about 1.5 to 2.5 cm/s. In contrast, the ambiguity velocity is not used in the Mode-8 velocity solver. The velocity in each bin is determined by auto-correlation, and Mode-8 admits a lower correlation threshold. Consequently, in Mode-8, the single-ping standard deviation for velocity measurement is about a factor of 10 greater than that of Mode-5. However, if de-correlation takes place in a bin, only the velocity in that bin is discarded, the remainder of the velocity profile is still considered valid, rendering less data lost. Although the standard deviation for single-ping measurements in Mode-5 is acceptable, potentially there could be more data dropouts than in the case of Mode-8 due to de-correlation. Thus, these two modes have their strengths and weaknesses. At the beginning of this study, it was not clear which mode of operation would be better suited for turbulence measurements. This question is to be addressed in this study.

Field deployments

The San Francisco Bay estuarine system, located between the Pacific Ocean at Golden Gate and the confluence of the Sacramento and San Joaquin Rivers, is one of the most complex coastal plain estuaries on the west coast of the United States. The San Francisco Bay system comprises Suisun Bay, San Pablo Bay, Central Bay, and South Bay. The bay system is typically identified as the northern reach (San Pablo, Suisun, and the northern part of San Francisco Bay to the Golden Gate) and the southern reach (San Francisco Bay south of Golden Gate), Fig. 2. The southern reach of San Francisco Bay is commonly referred to as South Bay, which is characterized as a tidal embayment with a main shipping channel (depth greater than 10 m) and large expansive shoal regions (depth $\approx$ 2 m). Hydrodynamic properties of South Bay vary seasonally and are controlled by tides, winds and freshwater inflows. Tides in the bay are mixed semidiurnal and diurnal, mainly semidiurnal, with pronounced spring neap variations; tidal amplitudes at spring tide can be twice those at neap tide. Tides propagate as a standing wave in South Bay; there is significant amplitude increase to the south (Cheng *et al.*, 1997, 1998). Because the dynamics of the bottom boundary layer may be affected by many factors including wind-wave interactions, influence of stratification, and unsteady tidal flow, the sites for the present study were deliberately chosen to have simple physical settings to minimize complications

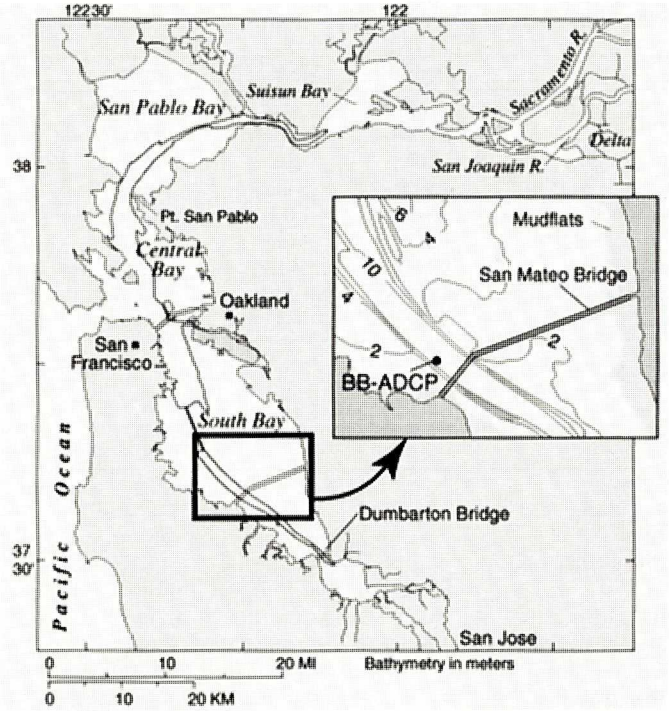

Fig. 2. Map of the study site in South San Francisco Bay, California.

in hydrodynamic characteristics due to complex bathymetry and salinity stratification. Thus, the primary forcing of the hydrodynamic bottom boundary layer in the present study was restricted to baratropic tidal currents only.

On October 15, 1997, two RDI BB-ADCPs (1200 kHz) were deployed in South Bay about 1 km south of the Dumbarton Railroad Bridge (Fig. 2). The main objective for this deployment was to evaluate and compare the two high-resolution modes of the BB-ADCP (Mode-5 and Mode-8) for measurements of turbulence properties in the bottom boundary layer. Characteristics of the two high-resolution modes and a more robust, but lower resolution Mode-4 are summarized in Table 1. The two BB-ADCPs were moored on the same platform, (Fig. 1), with transducers pointing downward and located at approximately 2 m above bed. The water depth at the deployment site is about 7 m. A 4-beam BB-ADCP was programmed to sample in Mode-5 and a 5-beam BB-ADCP was programmed to sample in Mode-8 at maximum sampling rate. Vertical resolution (bin size) for the 4-beam and 5-beam BB-ADCPs was 5 cm and 6 cm, respectively. Both ADCPs were programmed to sample in a burst-sampling strategy in which the instruments took 316 single-ping velocity profiles at their maximum sample rate (about 1 Hz for the 5-beam ADCP in Mode-8 and 1.4 Hz for the 4-beam

Table 1. Modes of BB-ADCP operations (RDI)

	Mode 4	Mode 5	Mode 5	Mode 8
# of beams	4	4	5	4
Frequency	1200 kHz	1200 kHz	1200 kHz	1200 kHz
Beam angle	20°	20°	20°	20°
Min. bin size	25 cm	5 cm	6 cm	5 cm
Min. depth of water	6.0 m	2.0 m	2.0 m	1.0 m
Max. range	~25 m	~4 m	~4 m	~4 m
Sampling rate	1.4 Hz	1.4 Hz	1.2 Hz	1.0 Hz
Single-ping standard deviation	~13 cm/s	~1 cm/s	~1 cm/s	~15 cm/s
De-correlation	No	$V >$ ~45 cm/s	$V >$ ~45 cm/s	$V >$ ~45 cm/s

Table 2. San Mateo Bridge deployment (Jan. 22–27, 1998)

Mode	5	5
# of beams	4	5
Burst	256	256
Sample frequency	~1.4 Hz	~1.2 Hz
Δt	30 min	30 min
Bin size	5 cm	6 cm
Single-ping standard deviation	~1 cm	~1 cm
De-correlation	$V >$ ~40–45 cm/s	$V >$ ~40–45 cm/s
Water depth	~14 m @ MLLW	~14 m @ MLLW
Last good bin to bed	7 cm	13 cm
Max. range	~4 m	~4 m

ADCP in Mode-5). The BB-ADCPs then slept for the remainder of the 15-minute burst-sample cycle. All individual velocity profiles were saved without averaging; they were downloaded from the instrument after recovery for further data analysis.

Between January 22 and January 27, 1998, a four-day deployment was carried out in the main shipping channel of South Bay about 1 km north of the San Mateo Bridge (Fig. 2). The water depth at the deployment site is about 14.5 m. Surface wind waves are not expected to penetrate to the bottom at that depth. In this deployment, two BB-ADCPs (a 4-beam and a 5-beam) were mounted in a similar downward-pointing configuration (Fig. 1). Both ADCPs were setup to sample in Mode-5 for a burst of 256 single-ping velocity profiles at a 30-minute burst-cycle. By recording every single-ping velocity profile, the sampling rate for the 4-beam system is about 1.4 Hz, and the sampling rate for the 5-beam system is about 1.2 Hz. The burst intervals for the two ADCPs were staggered by 15 minutes to avoid possible acoustic interference between the two instruments. The instrument setups for the January 22–27, 1998 deployment are summarized in Table 2. Both instruments successfully recorded time-series of velocity data that spanned about four days.

RESULTS

Preprocessing of time-series data

The ADCP measurements produce time-series of velocity bursts, with each burst representing a measurement point in the time-series from which the mean flow and turbulence properties are deduced. However, the time-series of single-ping velocity bursts are somewhat noisy; they must be screened for outliers before further analysis. Following Stacey (1997), the mean and standard deviation of data within each burst are computed. Any single-ping velocity that exceeds three standard deviations is considered an erroneous outlier which is removed from the burst. This process is carried out using the along beam direction velocities. The screening process for removing outliers repeats until all remaining data in a burst satisfy the criterion that each data point is less than three standard deviations. In periods with little de-correlation, less than 1 or 2% of the data are typically removed. If there are more than 20% erroneous data in a burst (typically due to de-correlation), that burst of data is discarded from the time-series. After the initial screening, these single-ping velocity burst time-series are used as the basis for computations of the mean flow and turbulence properties. A time-series of mean ADCP velocity profiles can be obtained by a straightforward averaging within each burst. This mean flow time-series is used for deductions of the bottom boundary layer properties.

Mean flow properties in the bottom boundary layer

To facilitate computations of turbulence properties, the original single-ping velocity data are saved as the along beam-direction velocities. As shown in Fig. 1, beams 1 and 2 of the ADCP are situated in the x-z plane, while beams 3 and 4 are in the y-z plane, with the z-axis pointing vertically down making a right-handed Cartesian coordinate system. The along beam velocities at a particular level are related to the earth coordinate velocity components by

$$V_{1j} = -u_{1j}\cos\theta - w_{1j}\sin\theta, \tag{1a}$$

$$V_{2j} = u_{2j}\cos\theta - w_{2j}\sin\theta, \tag{1b}$$

$$V_{3j} = -v_{3j}\cos\theta - w_{3j}\sin\theta, \tag{1c}$$

$$V_{4j} = v_{4j}\cos\theta - w_{4j}\sin\theta \tag{1d}$$

where the subscript j represents the j-th instantaneous measurement in the burst; (u, v, w) are the velocity components along the (x, y, z) directions; the indices 1, 2, 3, and 4 show the respective variable defined by beam 1, 2, 3, or 4. The angle θ is between the ADCP beam and the horizontal plane, in this case $\theta = 70°$.

By assuming that the flow properties within the spread of the ADCP beams

are statistically homogeneous, then the mean velocity components in earth coordinates should be the same when they are derived from statistical averaging of different instantaneous beam-values. Specifically, $\bar{u} = \bar{u}_1 = \bar{u}_2$, $\bar{v} = \bar{v}_3 = \bar{v}_4$, $\bar{w} = \bar{w}_1 = \bar{w}_2 = \bar{w}_3 = \bar{w}_4$, where an over-bar indicates that the variable is a statistically averaged value within a burst. In these measurements, the maximum spread between beams is less than 1.2 m, and this spatial homogeneity assumption is deemed reasonable and well accepted by the ADCP user community. Under this assumption, the ensemble averaged beam velocities (time-averaged beam velocities within a burst) can be written as:

$$\bar{V}_1 = -\bar{u}\cos\theta - \bar{w}\sin\theta, \tag{2a}$$

$$\bar{V}_2 = \bar{u}\cos\theta - \bar{w}\sin\theta, \tag{2b}$$

$$\bar{V}_3 = -\bar{v}\cos\theta - \bar{w}\sin\theta, \tag{2c}$$

$$\bar{V}_4 = \bar{v}\cos\theta - \bar{w}\sin\theta \tag{2d}$$

where an over-bar indicates a statistically averaged value. Therefore, the mean velocity components in earth coordinates, $u(z)$ and $v(z)$, can be obtained from Eq. (2) as

$$\bar{u}(z) = \frac{\overline{V_2(z)} - \overline{V_1(z)}}{2\cos\theta} \quad \text{and} \quad \bar{v}(z) = \frac{\overline{V_4(z)} - \overline{V_3(z)}}{2\cos\theta}. \tag{3}$$

Although the vertical velocity can be independently defined by beam 1 and 2 or by beam 3 and 4, a mean value is used so that

$$w(z) = -\sum_{i=1}^{4} \frac{\bar{V}_i(z)}{4\sin\theta}. \tag{4}$$

This redundancy in the vertical velocity is used to define an error velocity which gives a rough estimate of spatial homogeneity. The error velocity is defined as

$$\bar{\varepsilon} = \frac{\bar{V}_3 + \bar{V}_4 - (\bar{V}_1 + \bar{V}_2)}{2\sin\theta}. \tag{5}$$

Small values of error velocity are indications of consistency between the independently determined vertical velocity from beams 1 and 2 and from beams 3 and 4. This consistency check also implies spatial homogeneity in the statistical

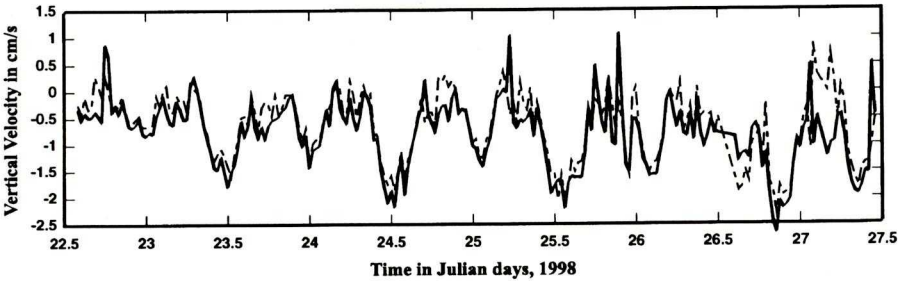

Fig. 3. Comparison of the vertical velocities estimated by a 4-beam BB-ADCP (dash line) and the vertical velocity measured by a 5-beam BB-ADCP (solid line) at about 80 cm above bed.

sense within the time span of a burst. Large error velocity suggests the possible violation of the spatial homogeneity assumption. In the 5-beam system, the 5-th beam is pointing vertically down, thus $w(z)$ is measured directly. As shown in Fig. 3, the estimated vertical velocity at bin-10 (~80 cm above bed) is compared to the directly measured w-velocity at the same distance from bed. In these measurements, the error velocities are quite small. The good agreement in vertical velocities and small error velocity values suggest that the spatial homogeneity is a reasonable assumption.

Although the single-ping velocity profiles measured with Mode-5 and with Mode-8 are substantially different, there is no significant difference between the Mode-5 and Mode-8 measurements after averaging (mean flow properties). After initial screening for outliers, the Mode-5 data show substantially larger amount of data drop-outs due to de-correlation than do those data obtained with Mode-8. On the other hand, the single-ping standard deviation in the Mode-8 data is nearly an order of magnitude greater than that for the Mode-5 data. While the turbulence fluctuation velocity is expected to be on the order of 1 cm/s, the noise to signal ratio in Mode-8 data is too large to allow extraction of meaningful turbulence variables from the Mode-8 data set in the configuration used in the present deployment. This analysis suggests that Mode-8 is not suitable for turbulence measurements in the bottom boundary layer. Therefore, in the following, only the data sets using Mode 5 from the January 22–27, 1998 deployment are presented and discussed.

Some ancillary data were also collected during the January 22–27, 1998 deployment. Figure 4 shows time-series of barometric pressure, salinity, total suspended solids, and water level (tides). Following Cheng *et al.* (1999), a global method is used to estimate values of z_0 and u_*. In the global method for bottom boundary layer analysis, a group of velocity profiles, which represent the bottom boundary layer flows within a short period of time (usually a few hours in this application), is considered simultaneously. Within this short time span, the sediment bed roughness is assumed to remain unchanged, and therefore there will

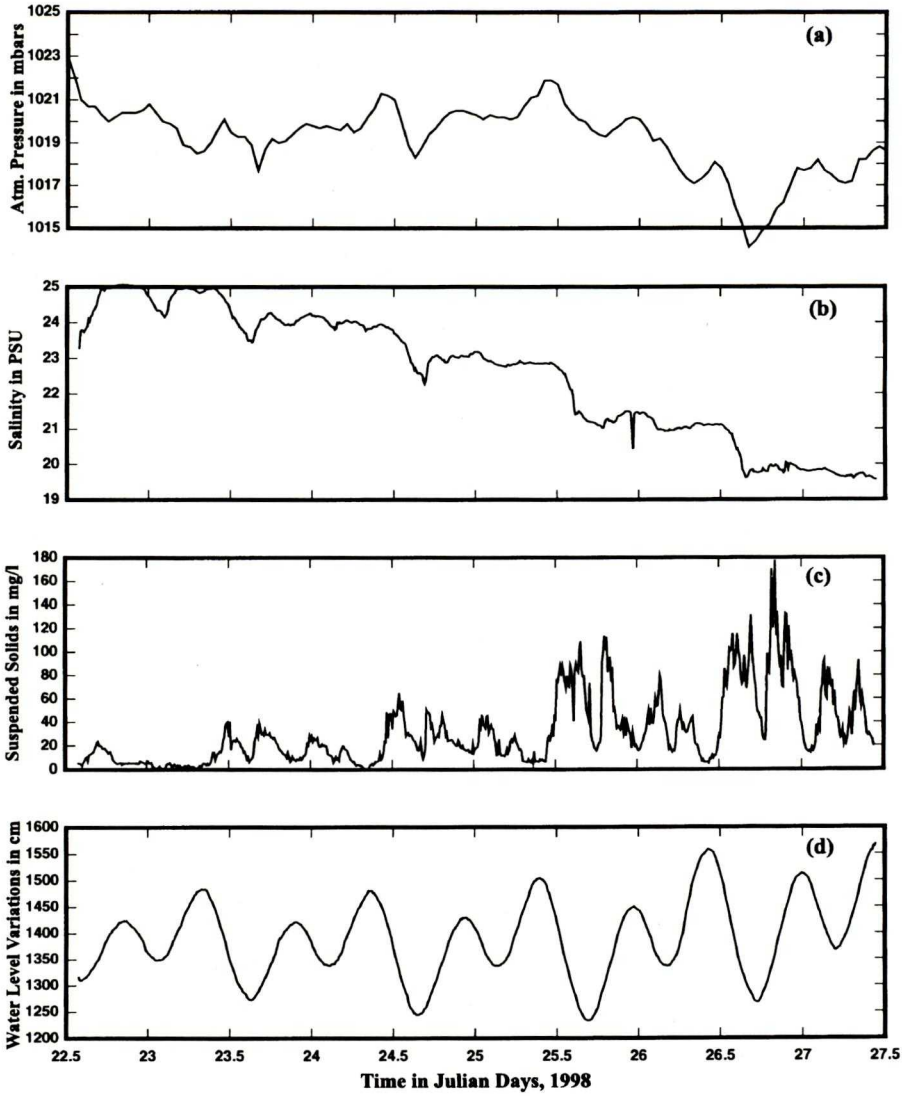

Fig. 4. The time-series of (a) barometric pressure, (b) salinity, (c) total suspended solids and (d) water level (tides) at the study site during the January 22–27, 1998 deployment.

be only one representative value of the bed roughness length for the time interval. Thus, when fitting this group of velocity profiles to the assumed logarithmic velocity distribution according to the "law of the wall", one z_0 for the entire interval along with values of u_* for each velocity profile included in this group are solved concurrently. Cheng *et al.* (1999) have shown the deduced boundary layer properties are more accurate and consistent. Using the global method, the

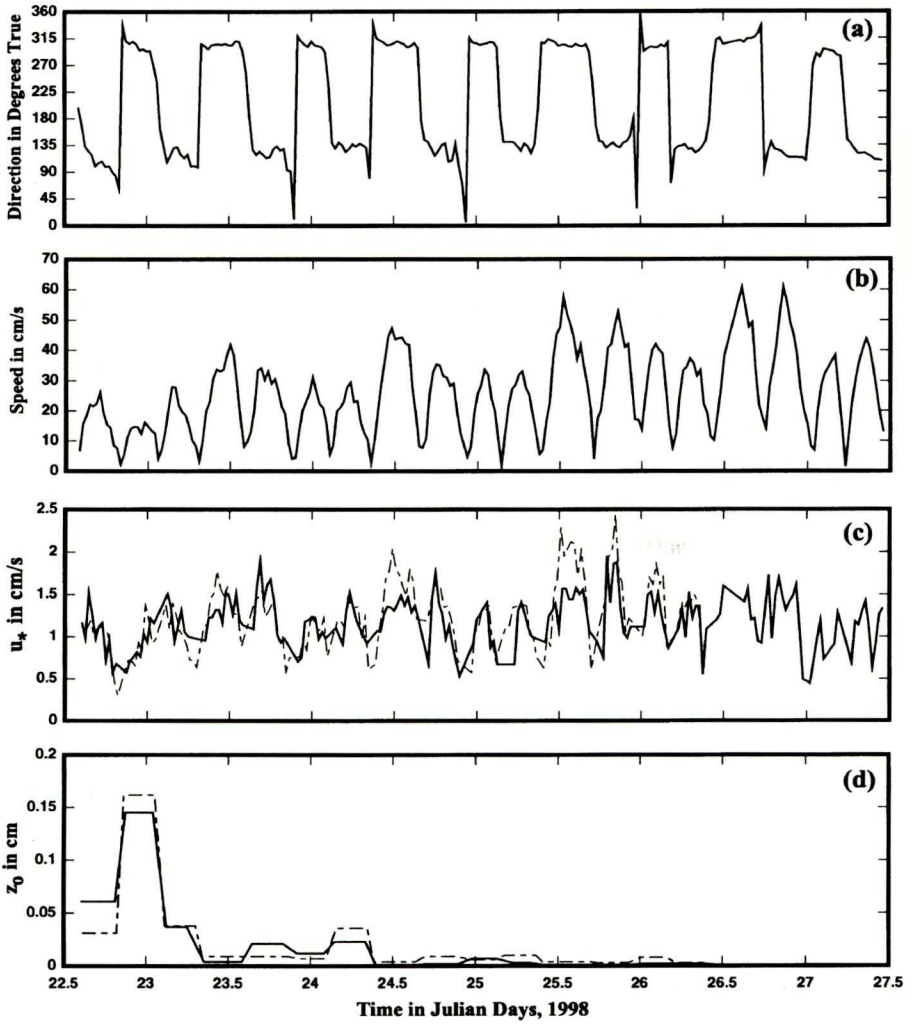

Fig. 5. The time-series of the tidal current (a) direction, (b) speed, (c) deduced friction velocity, u_*, (d) estimated roughness length, z_o. In (c) and (d), solid lines are the results derived from the 5-beam BB-ADCP and the dash lines are for the 4-beam BB-ADCP.

deduced u_* and z_o are plotted and presented in Fig. 5 along with the time-series of the speed and direction of tidal current at bin-5 (~115 cm above bed). As discussed in Cheng *et al.* (1999), occasional loss of some velocity profiles due to de-correlation of signal in Mode-5 tends to underestimate the magnitude of tidal velocity, $u(z)$, which may give rise to a slight bias error in roughness length in that the estimated z_o would be slightly higher. The estimated mean values for u_*, and z_o are about 1.22 cm/s and 0.02 cm at the San Mateo Bridge site. These values are

consistent with values obtained from previous measurements (Cheng *et al.*, 1999). The time-series of the estimated z_0 and u_* and mean speed and direction of tidal currents from both the 4-beam and 5-beam ADCP data are compared in Fig. 5 showing good agreement even for the deduced values of z_0 and u_*.

Turbulent properties in the bottom boundary layer

(a) Reynolds stress

Lohrmann *et al.* (1990) suggested that the Reynolds stress can be deduced from time-series of single-ping ADCP data by computing the cross-correlation of opposite pairs of velocities measured by the ADCP without the direct knowledge of individual velocity components. If the cross-correlation computations are deemed valid and the computations are carried out for each vertical level, the final result is a vertical distribution of the Reynolds stress. Two questions are of particular interest in this investigation: 1) What is the vertical Reynolds stress distribution? and 2) Does the Reynolds stress approach the bottom shear stress value near the bed?

Since the instantaneous velocity is a linear sum of the mean velocity and the fluctuating velocity, subtracting the mean from the instantaneous velocity in Eq. (1) gives the fluctuating velocity. Following the same notation as defined before, fluctuating beam velocities are given by

$$V'_{1j} = -u'_{1j}\cos\theta - w'_{1j}\sin\theta, \tag{6a}$$

$$V'_{2j} = u'_{2j}\cos\theta - w'_{2j}\sin\theta, \tag{6b}$$

$$V'_{3j} = -v'_{3j}\cos\theta - w'_{3j}\sin\theta, \tag{6c}$$

$$V'_{4j} = v'_{4j}\cos\theta - w'_{4j}\sin\theta \tag{6d}$$

where the fluctuating velocities are indicated as the primed quantities. Squaring Eqs. (6a), (6b), (6c), and (6d), using algebraic manipulations and the assumption of spatial homogeneity leads to expressions for the Reynolds stresses as

$$-\overline{u'w'}(z) = \frac{\overline{V'^2_2}(z) - \overline{V'^2_1}(z)}{2\sin 2\theta} \quad \text{and} \quad -\overline{v'w'}(z) = \frac{\overline{V'^2_4}(z) - \overline{V'^2_3}(z)}{2\sin 2\theta} \tag{7}$$

where $-\overline{u'w'}(z)$ is the Reynolds stress in the x-direction at z-level (referenced to ADCP bins) and $-\overline{v'w'}(z)$ is the Reynolds stress in the y-direction at z-level. The Reynolds stress is given as the correlations of the measured velocities. While the individual velocities measured at four beams separated by a distance on the order of one meter could be quite different, the statistical properties are assumed to be

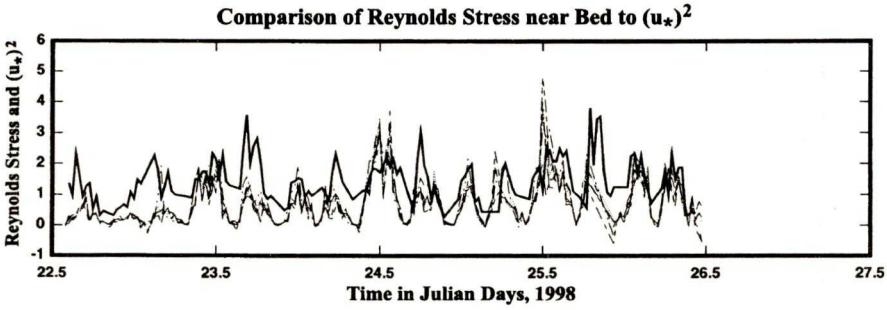

Fig. 6. Comparison of the time-series of bed shear stress, (u_*^2), shown as solid line with the computed Reynolds stress in bins 20–25 (10–40 cm from bed), dash lines. The units for (u_*^2) and for Reynolds stress are (cm/s)^2.

spatially homogeneous. This is equivalent to the assumption that the turbulence properties are homogeneous within the spatial scale represented by the spread of the ADCP beams. This assumption seems to be reasonable and has been also invoked by Stacey (1997) and Lu (1998) in their studies. The expressions given in Eq. (7) are for one bin level. Since the ADCP is capable of measuring velocity at many bins (or distances) from the bed, Eq. (7) can be generalized to give the vertical distribution of the Reynolds stress.

Analytically, the Reynolds stress near the bed approaches the value of the bottom shear stress. To validate the computed Reynolds stress distribution, it is compared to the bottom shear stress deduced independently from the mean flow velocity profiles. The deduced values for u_* and z_0 from the two BB-ADCPs (4-beam and 5-beam) are in very good agreement in general and are within the error bounds of the methods used for extracting u_* and z_0, Fig. 5. Thus, the bottom shear stress can be expressed in terms of u_* as $\tau_b/\rho = u_*^2$ in which u_* is derived from mean velocity profiles. The time-series of u_*^2 (solid line) from the 5-beam ADCP is compared with the time-series of Reynolds stress computed for the first six bins near bed (between 10 to 40 cm), Fig. 6. The comparison between the u_*^2 and the computed Reynolds stress obtained by the 4-beam BB-ADCP is also carried out, and the results are similar (not shown).

The Reynolds stresses in the first six bins near bed have nearly the same values throughout the 4-day deployment (Figs. 6 and 7). This observation suggests that the boundary layer near the bed is a constant shear layer. In a fully rough turbulent boundary layer, in order to arrive at a logarithmic velocity profile, the shear stress in this layer has been assumed to be constant (Schlichting, 1968). The Reynolds stress deduced from the present measurements is consistent with the constant shear stress approximation. Furthermore, as previously stated, the Reynolds stresses deduced from the two ADCP data sets compare extremely well with each other (not shown). These properties indirectly imply the validity of the direct measurements of the Reynolds stress in the bottom boundary layer

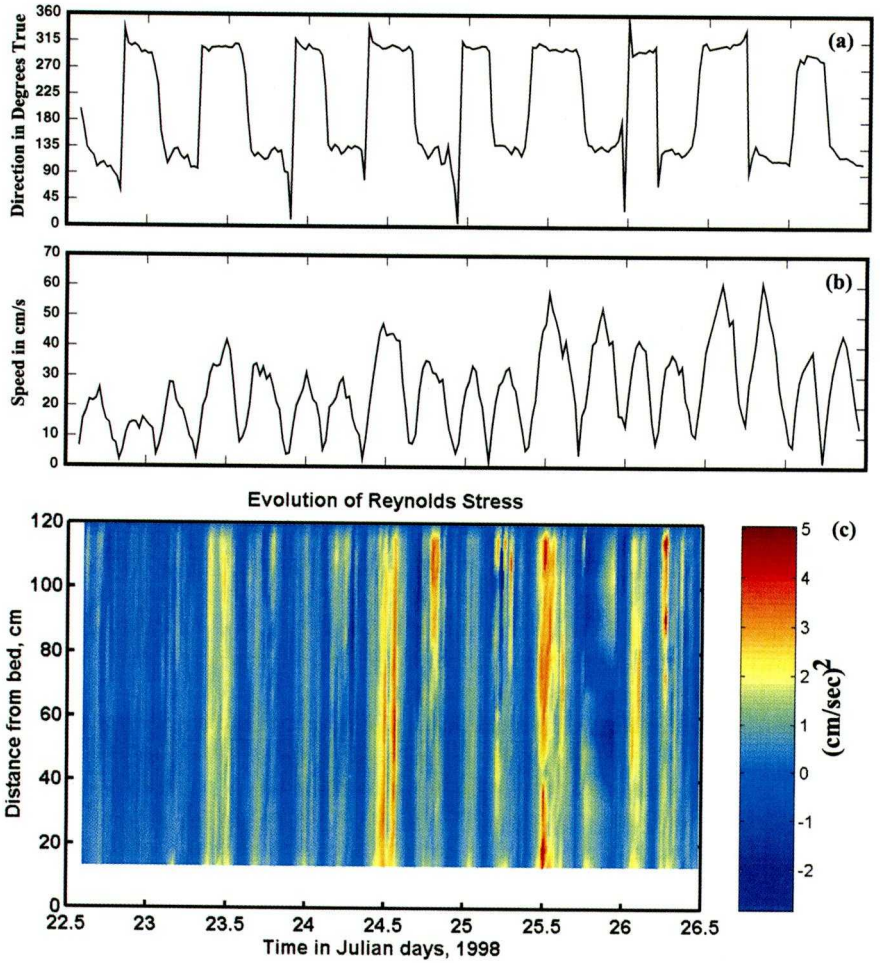

Fig. 7. Time-evolution of the Reynolds stress in the water column near bed. The top panels show the time-series of (a) tidal current direction and (b) speed which correlate with (c) the evolution of the Reynolds stress in time. The magnitude of the Reynolds stress is color coded in units of $(cm/s)^2$.

using BB-ADCPs. The bottom shear stress ($\tau_b/\rho = u_*^2$), represented by the solid line in Fig. 6, compares quite well with the Reynolds stress (other lines) close to the bed in the 4-day time-series. The maximum difference between u_*^2 and the Reynolds stress is less than 1 $(cm/sec)^2$. The cause of this difference between u_*^2 and the Reynolds stress is not clear. It is reasonable to assume that the differences are due to inherent errors in the Reynolds stress calculations and in the bottom shear stress (u_*^2) derivations. From these comparisons, the maximum error for the measured Reynolds stress is estimated to be about 1 $(cm/sec)^2$. These properties

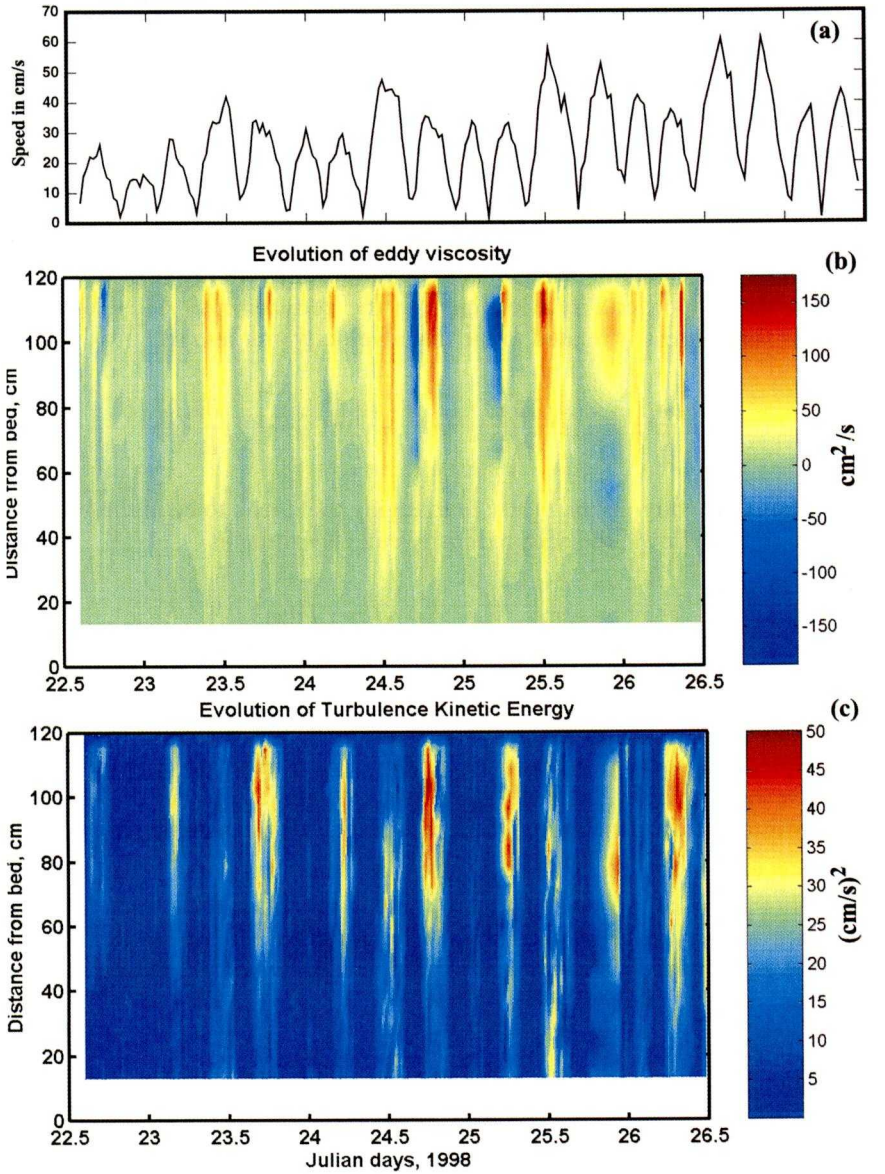

Fig. 8. (a) Time-series of tidal current speed, (b) time-evolution of eddy viscosity in cm^2/s, and (c) turbulent kinetic energy in $(cm/s)^2$ in the water column near bed.

prevail over the 4-days, as shown in the time evolution of the Reynolds stress in the water column near bed, Fig. 7. As the tidal currents evolve over the tidal cycles, the intensities of the Reynolds stress respond by changing values, but the vertical variance is generally absent. Throughout the tidal cycles, the bottom boundary layer basically remains a constant shear layer. As the tidal current speed intensifies, the respective value of Reynolds stress increases, and as the tidal velocity weakens approaching slack, the values of Reynolds stress diminish.

(b) Vertical eddy viscosity and turbulent kinetic energy

From these high frequency ADCP measurements, some additional turbulence properties can be extracted. Of particular interest is the vertical eddy viscosity which controls the dynamics of mixing in the water column. In general, the shear stress in the water column is assumed to be proportional to the vertical velocity gradient; the proportionality coefficient is the eddy viscosity. Therefore the Reynolds shear stress is related to the mean velocity gradient by

$$-\overline{u'w'}(z) = \varepsilon(z)\frac{\partial \bar{u}}{\partial z}(z) \quad \text{and} \quad -\overline{v'w'}(z) = \varepsilon(z)\frac{\partial \bar{v}}{\partial z}(z) \tag{8}$$

where $\varepsilon(z)$ is the eddy viscosity. By rearranging the x-axis to be in the principal direction of tidal flows, the eddy viscosity can be written as

$$\varepsilon(z) = (\text{Reynolds shear stress}) \Big/ \frac{\partial \overline{u_p}}{\partial z}(z) \tag{9}$$

where $\overline{u_p}(z)$ is the mean velocity profile in the principal tidal current direction. In principle, Eq. (9) can be used for evaluating $\varepsilon(z)$ in which the Reynolds stress and the vertical velocity gradient are known. Unfortunately, the resulting eddy viscosity is too noisy to make any sense in part due to the inaccuracy in the finite-difference expression for $\partial \overline{u_p}/\partial z(z)$. On the other hand, the mean velocity profiles fit the law-of-the-wall fairly well, and the computed shear stress is nearly constant, a property that associates with the logarithmic velocity profile. Thus, by using the logarithmic velocity profile, the vertical velocity gradient can be written as

$$\frac{\partial \overline{u_p}}{\partial z}(z) = \frac{u_*}{\kappa z} \tag{10}$$

and the eddy viscosity is given as

$$\varepsilon(z) = -\overline{u'w'}(z)\frac{\kappa z}{u_*}. \tag{11}$$

The computed eddy viscosity varies linearly with z, since the Reynolds stress is nearly constant as can be seen from Eq. (11). The eddy viscosity also varies with the changing tidal current speed. Generally, maximum values of eddy viscosity are found at maximum flood or ebb currents giving an eddy viscosity value of about 40–50 cm^2/s at 50 cm above bed. Near slack water, the values of eddy viscosity diminish. The time evolution of the eddy viscosity in the water column within the bottom boundary layer is shown in Fig. 8 (middle panel).

The turbulent kinetic energy distribution can be investigated using these high frequency ADCP data. The turbulent kinetic energy is defined as

$$\text{K.E.}(z) = 1/2[(u')^2 + (v')^2 + (w')^2] \tag{12}$$

where u', v', and w' are the turbulent fluctuation velocity components. The mean velocity in the vertical is assumed to be zero, thus the vertical turbulent fluctuation velocity is the same as the measured w-velocity. As shown in Fig. 3, the directly measured vertical velocity component appears to be valid. All quantities in Eq. (12) can be evaluated by using values of the measured along-beam velocities in Eq. (6). The resulting turbulent kinetic energy evolution over four days is shown in Fig. 8. In general, the turbulent kinetic energy is also roughly constant near bed. In steady open-channel flows and in the spatial scale over the depth of the channel, the turbulent kinetic energy distribution shows an increasing trend near the bed (Nezu and Nakagawa, 1993; Stacey and Monismith, 1998). While this trend holds true at a distance away from bed, some detailed measurements made by Wang and Qian (1989) suggest that in the layer very close to bed (within 10% of total water depth), the turbulent kinetic energy could be nearly constant. At this time, it is difficult to validate or invalidate the measured turbulent kinetic energy distribution. This is certainly an area of interest for further investigation.

DISCUSSION AND CONCLUSION

Direct measurements of mean flow and turbulence properties in the bottom boundary layer have been made using BB-ADCPs operating in high-resolution modes. There are advantages and disadvantages in both Mode-5 and Mode-8 operations of BB-ADCP; the choice of which mode is appropriate in a specific application involves a decision of compromise. In a series of field investigations, velocity data were measured using a burst sampling scheme in which the BB-ADCPs were programmed to record each single-ping velocity profile. Analysis of these data suggests that the mean flow properties obtained using either Mode-5 or Mode-8 are nearly identical. The single-ping standard deviation of velocity measurements in Mode-8 is an order of magnitude higher than that of Mode-5, rendering the noise to signal ratio in Mode-8 too high to be useful for turbulence measurements.

In a 4-day deployment in January 22–27, 1998, the high frequency velocity data were obtained for use in calculations of the Reynolds stress, eddy viscosity and turbulent kinetic energy distributions within the bottom boundary layer. The

Reynolds stress is found to be nearly constant in the bottom boundary layer, which is consistent with the constant shear assumption used in the derivation of logarithmic velocity profile. The eddy viscosity is shown to vary linearly with distance from bed. The magnitudes of both the Reynolds stress and eddy viscosity are well correlated with variations in tidal current speed throughout the tidal cycles. The computed turbulent kinetic energy is also nearly constant, although this finding is not conclusive.

Overall, this approach of using BB-ADCP for turbulence measurements has been a very useful exercise. If the instrument internal recording is not a limit, by saving each single-ping velocity measurement, all mean flow properties measured in conventional BB-ADCP applications can be recovered from the high-frequency data. There are certain hardware limitations inherent in the instrument that warrant further considerations and improvements in future studies. The fact that BB-ADCP might "de-correlate" limits this type of application to less energetic flows. In high frequency sampling modes, the data-sampling rate for RDI SC-1200 is limited to slightly above 1 Hz. This sampling rate is not quite sufficient to resolve the fine eddies in natural flows in estuaries. The physical size of the BB-ADCP and mounting frame are somewhat too bulky; there is a possibility that the instrument platform might be blocking the flows near the instrument. Nevertheless, the results from these initial attempts in using BB-ADCP for measuring detailed turbulence properties in the bottom boundary layer are quite encouraging. Further studies are being planned in which efforts will be made to reduce or eliminate these limitations identified in the present investigation. If these limitations can be minimized or removed, the BB-ADCP would be a suitable and powerful tool for studies of turbulence in estuarine and coastal seas.

Acknowledgements. The authors wish to thank Mark Stacey for many fruitful discussions during the course of this investigation.

REFERENCES

Cheng, R. T., J. W. Gartner and R. E. Smith (1997): Bottom boundary layer in South San Francisco Bay, California. *J. Coastal Research*, **SI-25**, 49–62.

Cheng, R. T., J. W. Gartner, D. A. Cacchione and G. B. Tate (1998): Flow and suspended particulate transport in a tidal bottom boundary layer, South San Francisco Bay, California. In *Physics of Estuaries and Coastal Seas*, edited by J. Dronkers and M. Scheffers, pp. 3–12, Balkema, Rotterdam.

Cheng, R. T., C.-H. Ling, J. W. Gartner and P. F. Wang (1999): Estimates of bottom roughness length and bottom shear stress in South San Francisco Bay, California. *J. Geophys. Res.*, **104**, No. C4, 7715–7728.

Gordon, R. L. (1996): *Acoustic Doppler Current Profiler, Principles of Operation—A Practical Primer*. RD Instruments, San Diego, CA, 54 pp.

Lhermitte, R. and U. Lemmin (1994): Open-channel flow and turbulence measurement by high-resolution Doppler sonar. *J. Atmos. Ocean. Technol.*, **11**, No. 5, 1295–1308.

Lohrmann, A., B. Hackett and L. P. Roed (1990): High resolution measurements of turbulence, velocity and stress using a pulse-to-pulse coherent sonar. *J. Atmos. Ocean. Technol.*, **7**, 19–37.

Lu, Y. (1998): Flow and turbulence in a tidal channel. Ph.D. Thesis, University of Victoria, British of Columbia, Canada, 140 pp.

Lueck, R. and Y. Lu (1997): The logarithmic layer in a tidal channel. *Continental Shelf Research*, **17**, No. 14, 1785–1801.

Nezu, I. and H. Nakagawa (1993): *Turbulence in Open Channel Flows*. A. A. Balkema, 281 pp.

RD Instruments (1997): RD Instrument Acoustic Doppler Current Profilers, DR/SC Technical Manual, March 1997, RD Instruments, San Diego, CA, 378 pp.

Schlichting, H. (1968): *Boundary Layer Theory*. 6-th ed., McGraw Hill, 744 pp.

Stacey, M. T. (1997): Turbulent mixing and residual circulation in a partially stratified estuary. Ph.D. Thesis, Stanford University, Stanford, California, 207 pp.

Stacey, M. T. and S. G. Monismith, (1998): *Measuring Estuarine Turbulence with an ADCP*. The 27th Congress, IAHR, August 1998, San Francisco, CA, 155–160.

Wang, X. and N. Qian (1989): Turbulence characteristics of sediment-laden flow. *J. Hydraulic Engineering, ASCE*, **115**, No. 6, 781–800.